A study on the predawn ionospheric heating effect and its main controlling factors

Zhenzhang Tang[1], Huijun Le[1], Libo Liu[2], Yiding Chen[1], Ruilong Zhang[1], Wenbo Li[1], and Wendong Liu[1]

[1]Institute of Geology and Geophysics, Chinese Academy of Sciences
[2]Key Laboratory of Earth and Planetary Physics, Institute of Geology and Geophysics, Chinese Academy of Sciences

April 12, 2024

Abstract

We proposed for the first time that the angle between the projection of the magnetic field line and the sunrise line (AMFS) is a crucial factor controlling predawn heating. Then, we quantitatively investigated the relationship between the predawn heating effect and the AMFS depending on the model results and examined the influence of the length of the magnetic field line (LMF). The results indicate that the predawn heating is influenced by the combined effect of the AMFS and the LMF. Our study suggests that the increase of AMFS promotes predawn heating, while the increase of LMF blocks predawn heating. Finally, we found that when the LMF is about 4000 km and the AMFS is around 30 degrees, the combined effect of the AMFS and the LMF on the predawn heating effect reaches its maximum, exceeding 400K, while the influence of both AMFS and LMF exhibit saturation effects.

A study on the predawn ionospheric heating effect and its main controlling factors

Zhenzhang Tang[1,2,5], Huijun Le[1,2,3,5], Libo Liu[1,2,3,5], Yiding Chen[1,2,4,5], Ruilong Zhang[1,2,3,5], Wenbo Li[1,3], Wendong Liu[1,2,5]

[1] Key Laboratory of Earth and Planetary Physics, Institute of Geology and Geophysics, Chinese Academy of Sciences, Beijing, 100029, China

[2] Institutions of Earth Science, Chinese Academy of Sciences, Beijing, 100029, China

[3] Heillongjiang Mohe National Observatory of Geophysics, Institute of Geology and Geophysics, Chinese Academy of Sciences, Beijing, 100029, China

[4] Beijing National Observatory of Space Environment, Institute of Geology and Geophysics, Chinese Academy of Sciences, Beijing, 100029, China

[5] College of Earth and Planetary Sciences, University of the Chinese Academy of Sciences, Beijing, 100049, China

Corresponding author: Huijun Le (lehj@mail.iggcas.ac.cn)

Key Points:

- A gridded empirical ion temperature model is constructed utilizing the Rocsat-1 observations.
- The angle between magnetic field line and sunrise line is proposed for the first time as a key factor controlling predawn heating.
- The combined effects of the angle between magnetic field line and sunrise line and the length of magnetic field line on predawn heating are quantitatively investigated.

Abstract: We proposed for the first time that the angle between the projection of the magnetic field line and the sunrise line (AMFS) is a crucial factor controlling predawn heating. Then, we quantitatively investigated the relationship between the predawn heating effect and the AMFS depending on the model results and examined the influence of the length of the magnetic field line (LMF). The results indicate that the predawn heating is influenced by the combined effect of the AMFS and the LMF. Our study suggests that the increase of AMFS promotes predawn heating, while the increase of LMF blocks predawn heating. Finally, we found that when the LMF is about 4000 km and the AMFS is around 30 degrees, the combined effect of the AMFS and the LMF on the predawn heating effect reaches its maximum, exceeding 400K, while the influence of both AMFS and LMF exhibit saturation effects.

1.Introduction

With the increased observational data from satellites, the study of the topside ionosphere has received more and more attention and has made significant progress. Plasma temperature is a critical parameter in ionospheric research, which significantly affects photochemical processes, transport processes and kinetic processes. The in-situ measurement of plasma temperature in the ionosphere using spacecraft instruments has a history of several decades [Hanson et al., 1970; Heelis and Hanson, 1980; Oyama et al., 1996a, 1996b; Venkatraman and Heelis, 1999]. Studying the plasma temperature of the ionosphere is essential for understanding the energy balance of the ionosphere and the nature of other physical processes.

Many scientists have developed empirical models of the ionosphere based on observations to describe the variations in plasma temperature (Brace and Theis, 1981; Kohnlein, 1986; V Truhlík, 2021, et al.). The solar extreme ultraviolet (EUV) radiation produces high-energy photoelectrons during the process of photoelectric ionization. Most of the remaining energy of photoelectrons is transferred to the background electrons by collisions. The electrons are heated, and the temperature rises. The electrons then transfer energy to the ions, which finally collide with the neutral gas to heat it. Therefore, the electron temperature (Te) is significantly higher than the neutral temperature (Tn), while the ion temperature (Ti) is usually somewhere in between (Banks and Kockarts, 1973).

Photoelectrons are the primary heating source in the ionosphere. Rapid cross-hemisphere transport of photoelectrons along magnetic field lines would cause some exciting changes, such as the conjugated hemispherical ionospheric response during eclipses (e.g., Le et al., 2008, 2010, 2020) and the predawn ionospheric heating effect (e.g., Kwei and Nisbet; Richards and Torr, 1986). Predawn heating refers to the scenario where, in certain longitudinal sectors, the winter hemisphere experiences a temperature increase before sunrise. The first report of predawn heating in the topside ionosphere was the observation at the Arecibo Ionospheric Observatory using incoherent scatter radar observations (Carlson, 1966). Chao et al. (2003) observed the ion predawn heating by analyzing data from the Rocsat-1 satellite. Kakinami et al. (2009) utilized data from the Hinotori satellite to study the predawn heating of the topside ionosphere under conditions of high solar activity and moderate geomagnetic disturbances. They calculated the beginning time and rate of the predawn ionosphere heating. Their findings indicated that the rate of predawn ionosphere heating decreased with increasing field line length. The heating rate remains relatively constant when the field line length increases to approximately 5000 km. Based on these studies, Chao et al. (2010) utilized the SAMI2 ionospheric model to reconstruct the temperature distribution and local time variations at an altitude of 600km. The SAMI2 model suggests that photoelectrons flowing along magnetic field lines from the solar-illuminated magnetic conjugated ionosphere footing are the primary heat source for the predawn plasma heating region.

Previous studies focused on the influence of the length of the magnetic field line (hereinafter referred to as LMF) between the magnetic conjugated points of the northern and southern hemispheres on the predawn heating. The relative position between the projection of the magnetic field line on the horizontal plane and the sunrise line should also be another essential factor. It is known that the Earth's magnetic field is not a simple tilted dipole field but has a more complex structure. Big magnetic declinations exist in some longitudinal sectors. Therefore, there is a significant difference in the geographical longitude of the magnetic field lines between the north and south magnetic conjugated points in different longitude sectors; that is, there is an angle between the projection of magnetic field lines and the geographic longitude lines. The sunrise line also exhibits a varying angle with the geographical longitude lines throughout the different seasons. At the equinoxes, this angle is zero, meaning that the sun rises at the same time in the northern and southern hemispheres at the same geographic latitude. This angle reaches the maximum in the November solstice or June solstice, and the sunrise in the winter hemisphere is significantly later than that in the summer hemisphere within the same meridian plane. Suppose the magnetic field lines approach parallelism with the sunrise line. In that case, no significant predawn heating will occur because the North and South

Hemispheres located on the same magnetic field line experience sunrise simultaneously, and the photoelectrons are generated simultaneously on both hemispheres. Conversely, suppose a significant angle that exists between the magnetic field line and the sunrise line (hereinafter referred to as AMFS). In that case, the photoelectrons generated in the hemisphere that experiences sunrise first can transport along the magnetic field lines to the conjugated hemisphere that has not yet experienced sunrise, thereby causing predawn heating.

In this study, we first constructed an ionospheric ion temperature model based on Rocsat-1 ion temperature data using the gridding method. Then, based on this model, we studied how the length of the magnetic field line (LMF) and the Angle between the projection of the magnetic field line and the sunrise line (AMFS) affect the predawn heating.

2. Observational data and ion temperature modeling

In this study, we constructed a global ion temperature empirical model based on the ion temperature data from the Rocsat-1 satellite from 1999 to 2004. The satellite's orbital inclination is approximately 35 degrees, covering a latitude range of ±35 degree, and its orbital altitude is between 560-660km. The Rocsat-1 satellite has accumulated over 15 million data points in six years. Because there is so much data, we use a grid modeling method to build a more accurate ion temperature model. All data are placed in fixed latitude and longitude grid points, which are 2 degrees apart at latitude and 7.5 degrees at longitude. We developed an ion temperature model for each grid that varied with solar flux F107, local time, seasons, and altitude. By assembling these grid models, we constructed an ion temperature model covering the global middle and low latitudes.

We conducted preprocessing on the observational data to establish a more accurate ion temperature model. First, to mitigate the influence of geomagnetic activity, we only utilized observational data with $Kp < 3$. There are also some irregularities in the topside ionosphere where ion density and temperature vary dramatically. Modeling of the ionosphere necessitates the exclusion of data from these irregularities. We employed a method based on ion density gradient detection and eliminated data with large gradients (e.g., Huang 2023), thereby reducing the impact of the irregularities.

After data processing, we allocated the ion temperature data into regular grids corresponding to their latitude and longitude coordinates. Averaging over six thousand data points in a grid were used to establish an ion temperature model for every grid. The Rocsat-1 satellite data covers a latitudinal range from -35.1 degrees to 35.1 degrees and a longitudinal range from 0 to 360 degrees. The model grid central points are divided latitudinally from -35° to 35° with a 2° interval, and longitudinally from 0° to 360° with a 7.5° interval. Therefore, the global middle and low latitudes are divided into 1728 (36×48) grid points. Each grid has a latitudinal width of ±2° and a longitudinal width of ±7.5°. Separate ion temperature models that vary with solar activity, season, local time, and altitude are established for each grid point. The model equation is as follows:

$$
\begin{cases}
\mathrm{Ti}_{\mathrm{global}} = \bigcup \mathrm{Ti}_{\mathrm{ij}}, \mathrm{Ti}_{\mathrm{ij}} = \mathrm{F}_1(\mathrm{F}_{107}) \cdot \mathrm{F}_2(\mathrm{Doy}) \cdot \mathrm{F}_3(\mathrm{LT}) \cdot \mathrm{F}_4(\mathrm{Altitude}) \\
\mathrm{F}_1(\mathrm{F}_{107}) = \mathrm{a}_0 + \mathrm{a}_1 \cdot \mathrm{F}_{107} + \mathrm{a}_2 \cdot {\mathrm{F}_{107}}^2 \\
\mathrm{F}_2(\mathrm{Doy}) = 1 + \sum_{\mathrm{i}=1}^{4} \mathrm{a}_{2\mathrm{i}+1} \cdot \cos\left(\frac{2\pi \cdot \mathrm{i} \cdot \mathrm{Doy}}{365}\right) + \sum_{\mathrm{i}=1}^{4} \mathrm{a}_{2\mathrm{i}+2} \cdot \cos\left(\frac{2\pi \cdot \mathrm{i} \cdot \mathrm{Doy}}{365}\right) \\
\mathrm{F}_3(\mathrm{LT}) = 1 + \sum_{\mathrm{i}=1}^{4} \mathrm{a}_{2\cdot \mathrm{i}+9} \cdot \cos\left(\frac{2\pi \cdot \mathrm{i} \cdot \mathrm{LT}}{24}\right) + \sum_{\mathrm{i}=1}^{4} \mathrm{a}_{2\mathrm{i}+10} \cdot \cos\left(\frac{2\pi \cdot \mathrm{i} \cdot \mathrm{LT}}{24}\right) \\
\mathrm{F}_4(\mathrm{Altitude}) = 1 + \mathrm{a}_{19} \cdot \mathrm{Altitude}
\end{cases}
$$

The $\mathrm{Ti}_{\mathrm{ij}}$ is an ion temperature model built on a fixed latitude and longitude grid (latitude i, i=1,..36; longitude j, j=1,..48). The F_1, F_2, F_3 and F_4 respectively represent the solar cycle variation, seasonal variation, local time variation, and altitude variation (e.g., A, E et al., 2012; Le et al., 2017; Xu & Kamide, 2004; Le et al., 2022; Huang et al., 2015;). For each grid model, we fit the above ion temperature model by non-linear least squares and calculate 20 coefficients, and our model has 34560 (1728*20) coefficients in total. Based on our model and these calculated coefficients, the global distribution of ion temperature for a given solar activity, season, local time/universe time, and altitude can be acquired.

3. Results and Discussion

To evaluate the model's performance, we compared the model values with the observations and calculated the error between the model results and the observations. Figure 1 illustrates the distribution of errors and the comparison of model values with observed values. The median error of the model is 58.6 K. The slope of the fitting line between the observed and model results is 1.0041. These results show that the empirical model fits the observed dataset very well. Subsequent model calculations are the result at altitude of 600km under moderate solar activity condition (F107=140).

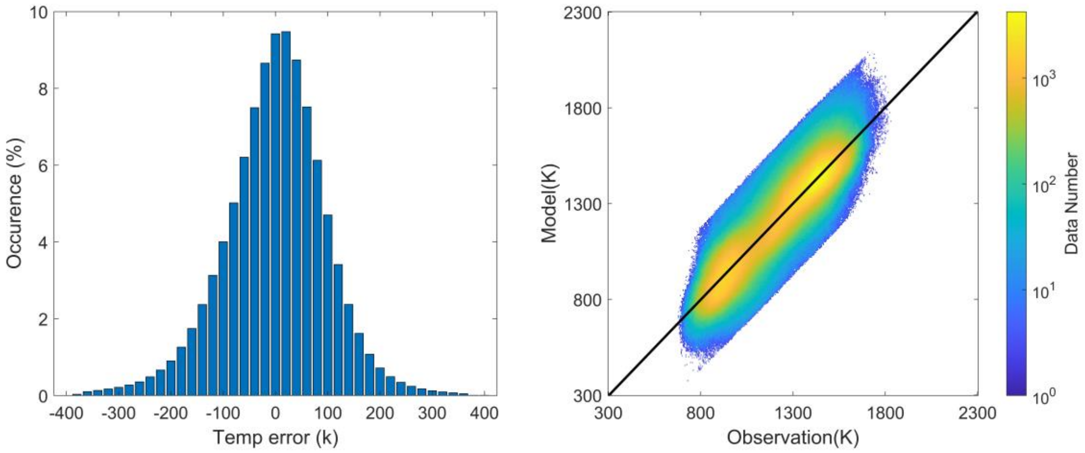

Figure 1. The left panel shows the ion temperature error, and the median error of the model is 58.6K. The right panel is the count bin figure, and the black line represents the fitting line between the observed and model results, with a slope of 1.0041.

In this study, the angle between magnetic field lines and sunrise lines, AMFS, is defined as the difference in geographical longitude between the footings of the magnetic field lines in the northern and southern hemispheres, minus the difference in geographical longitude between the sunrise lines at the corresponding geomagnetic latitudes, i.e.:

$$L_1 = L_{M1} - L_{M2}$$

$$L_2 = L_{R1} - L_{R2}$$

$$AMFS = L_1 - L_2$$

Wherein, L_1 represents the difference in geographical longitude between the footings of the magnetic field lines, L_{M1} and L_{M2} denote the corresponding geographical longitudes in the northern and southern hemispheres. L_2 represents the difference in geographical longitude between the sunrise lines at the corresponding geomagnetic latitudes, L_{R1} and L_{R2} denote the corresponding geographical longitudes in the northern and southern hemispheres. Figure 2d illustrates the definition and calculation of AMFS. Using the International Geomagnetic Field model (Alken et al., 2021), we first traced the magnetic field lines originated from different geomagnetic latitudes (ranging from 3° to 30°) in various longitudinal sectors at an altitude of 600 km. After that, we traced the magnetic field line to 200 km, so that the projection of magnetic field line and the sunrise line are on the same plane, getting the values of L_{M1} and L_{M2}. Then, we computed the position of the sunrise lines at an altitude of 200 km at the corresponding geomagnetic latitudes, getting the values of L_{R1} and L_{R2}. Finally, we can calculate the value of AMFS. At the same time, we also calculated the length of magnetic field lines from different magnetic latitudes. For the reason that the photoelectrons are mainly transported along the magnetic field line above 300 km, the calculation of the length of magnetic field lines retains the part of 300 km to 600 km in different hemisphere.

The intensity of predawn heating is defined as the difference between the ion temperature of the posterior sunrise hemisphere at sunrise and the anterior sunrise hemisphere at sunrise. Figure 2d illustrates the positions of two calculated points in the northern and southern hemispheres, and the intensity of predawn heating is calculated as $\Delta \mathrm{T} = (\mathrm{T_{A2}} - \mathrm{T_{A1}})$. T_{A2} represents the ion temperature at the A2 point at sunrise, and T_{A1} represents the ion temperature at the A1 point at sunrise.

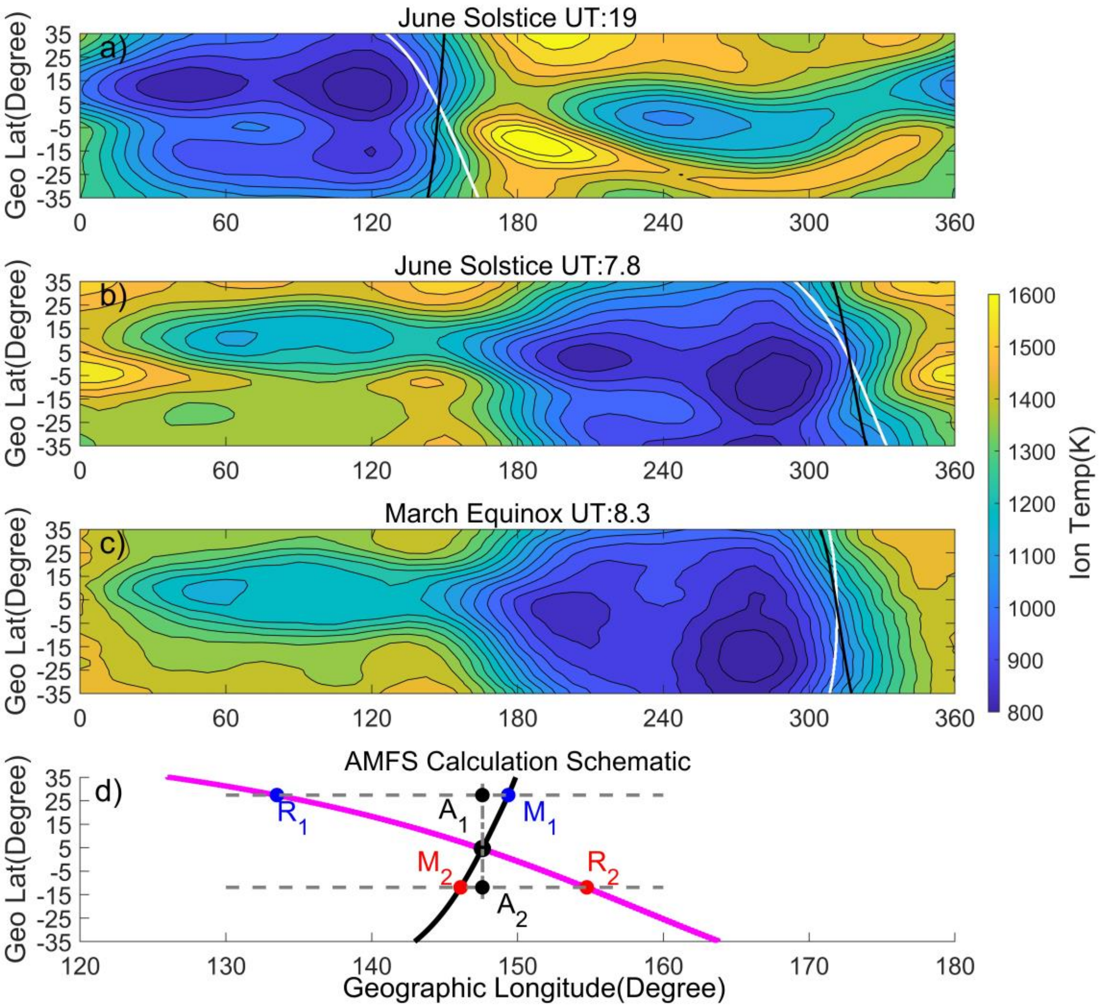

Figure 2. Figure 2a-c illustrates the global distribution of ion temperatures at certain Universal Time (UT) at the June solstice and March equinox, when the altitude is 600km and F107 is 140. Figure 2d elaborates the definition and calculation of AMFS. The magenta line is the sunrise line, and the black line is the magnetic field lines in the horizontal projection. L_{M1} and L_{M2} indicate the points of the same magnetic latitude in the northern and southern hemispheres. L_{R1} and L_{R2} indicate the position of sunrise at the corresponding magnetic latitude. A1 and A2 indicate the points at which predawn heating is calculated in the northern and southern hemispheres.

Figure 2a-c illustrates some examples of predawn heating of ion temperatures at the June solstice and March equinox. The relative position of the magnetic field lines in the horizontal projection (black lines) and the sunrise lines (white lines) are also shown in the figure. As shown in Figure 2a, the magnetic field line has a significant angle with the sunrise line, resulting in a considerable value of AMFS. Thus, we can see a significant increase in ion temperature at sunrise in the southern hemisphere. However, if the angle is significantly reduced (as shown in Figure 2b), the predawn heating effect is significantly reduced. The northern and southern hemispheres have the same sunrise time in the March or September equinoxes. Therefore, the predawn heating effect is usually not easy to occur. However, if the magnetic field line has enough deflection angle in some longitude sectors like 315° - 330°, the predawn heating effect can still be produced, as shown in Figure 2c.

The above results suggest that AMFS is indeed an essential factor affecting pre-dawn heating. Therefore, based on the empirical ion temperature model constructed above, we conducted a quantitative study to investigate the effect of the AMFS on predawn heating. Previous studies on the intensity of the predawn heating effect have primarily focused on the length of the magnetic field lines, suggesting that the heating rate decreases with the increase in LMF (Kakinami et al., 2009). Utilizing the ion temperature model constructed above, we have also quantitatively investigated the impact of LMF on the predawn heating effect. By employing the ion temperature model, we simulated the ion temperature at the global middle and low latitude topside ionosphere at 600km under moderate solar activity conditions on different days with day numbers ranging from 5 to 365, with an interval of 5 days.

Firstly, we examined the impact of the AMFS. Figure 3 illustrates the variation of ion temperature enhancement with AMFS at approximately the same LMF. For each panel, the data includes results within ± 10% of the center LMF. The red line in the figure represents the fitting line for the scatter points, with k being the slope of the fitting line. We have separately calculated their relationship of variation for different LMF ranging from 2000 km to 10000 km. The statistical results indicate that the AMFS value has an essential impact on the predawn enhancement in ion temperature. For the same LMF, the larger AMFS results in the greater ion temperature enhancement meaning stronger effect of predawn heating. The k value reflects the efficiency of AMFS's predawn heating. As the LMF increases, the k value gradually decreases. That is, for regions with longer magnetic field lines at higher latitudes, a larger AMFS would be required to achieve the same predawn ion temperature enhancement. This implies that the influence of the AMFS on the predawn ion temperature enhancement is reduced as LMF increases.

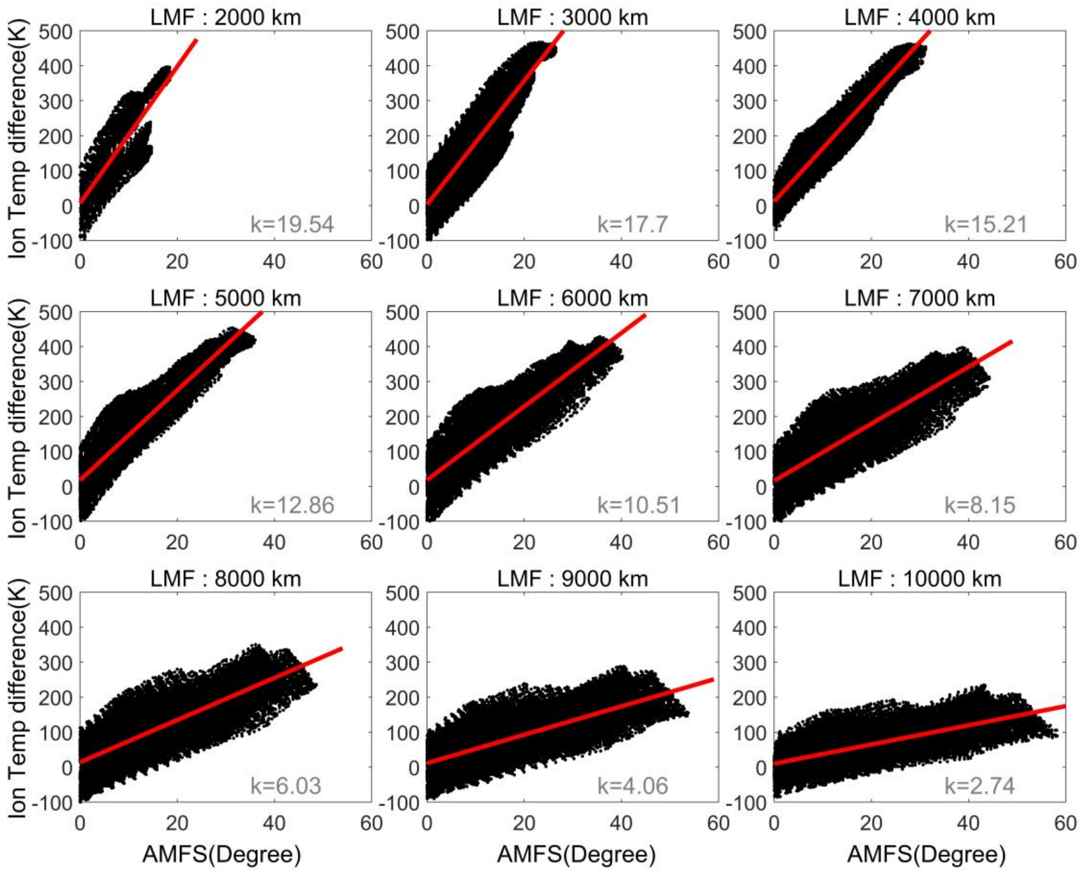

Figure 3. The relationship between AMFS and the temperature difference between the northern and southern hemispheres, within different ranges of LMF (from 2000-10000 km, with a span of plus or minus 10% before and after). The red line represents the fitting line, with k being the slope of the fitting line.

We further investigated the impact of LMF on predawn heating. Figure 4 illustrates the variation of predawn heating with LMF at the different AMFS values, ranging from 5 degrees to 45 degrees with a span of plus or minus 2.5 degrees before and after. Statistical results indicate that under conditions where AMFS is approximately the same, the longer the LMF is, the weaker the predawn heating effect is. The k absolute value reflects the efficiency of LMF blocking predawn heating. As the AMFS increases, the k absolute value gradually increases. That is, for longitudinal sectors and seasons with smaller AMFS, a shorter LMF would be required to achieve the same predawn ion temperature enhancement. This implies that the influence of the LMF on the predawn ion temperature enhancement is increased as AMFS increases. By comparing Figures 3 and 4, we can observe that both the correlation between the predawn heating effect and LMF and that between the predawn heating effect and

AMFS are strong, which suggest that the predawn heating effect is jointly controlled by the AMFS and AMFS.

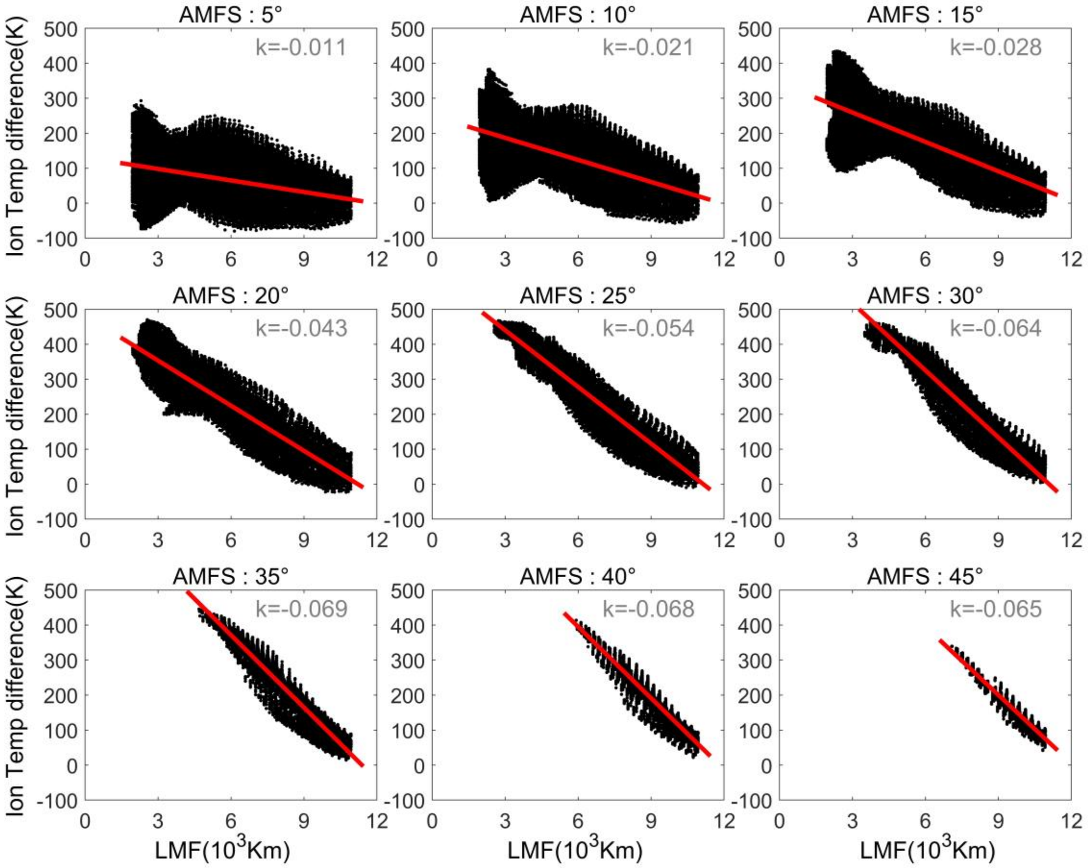

Figure 4. The relationship between the LMF and the temperature difference between the northern and southern hemispheres in different AMFS, and other descriptions are the similar as Figure 3.

As mentioned above, the predawn heating effect is influenced by both LMF and AMFS. The increase in LMF value decreases the predawn heating effect. The increase in AMFS value will increase the heating effect. In addition, with the increase of geomagnetic latitude, LMF will gradually become more prolonged for the same longitude sector, and AMFS will also become larger. To comprehensively consider the combined effects of LMF and AMFS on the ion predawn heating effect, we further calculated the average predawn heating effect under different conditions of LMF ranging in 2000 - 10000 km and AMFS ranging in 5° - 50°. Figure 5 presents a contour map showing the predawn heating as a function of LMF and AMFS. This result clearly shows how AMFS and LMF work together to influence predawn heating. We can find that the predawn heating effect is most significant when the AMFS value is about 30 degrees and the LMF value is around 4000 km, and the ion temperature increases by more than 400K. As the length of magnetic field lines increases, the strongest predawn heating occurs at larger AMFS values.

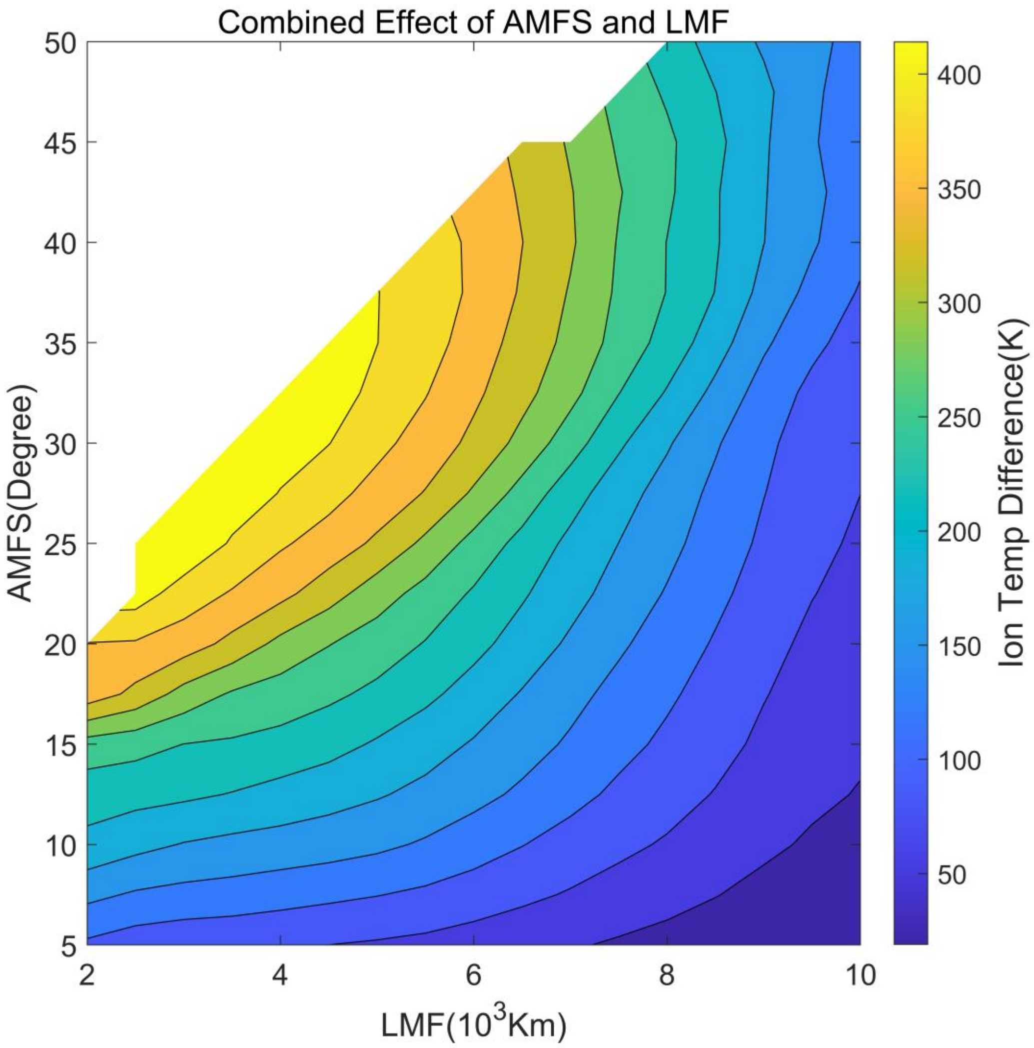

Figure 5. The combined effect of the LMF and AMFS on the predawn heating effect.

The AMFS reflects the difference in sunrise time at the northern and southern ends of the same magnetic field line. When AMFS approaches zero, the northern and southern hemispheres of the same magnetic field line experience sunrise simultaneously, regardless of whether the magnetic field line deviates from the geographical meridians. Conversely, when the AMFS value is bigger, there will be a difference in sunrise time between the northern and southern hemispheres of the same magnetic field line. Moreover, the larger the AMFS is, the greater the difference in sunrise time between the conjugated northern and southern hemispheres along the magnetic field line is. This will result in the photoelectrons from the hemisphere that experiences sunrise first are able to transport along the magnetic field line to the conjugated hemisphere earlier, thereby causing earlier and longer-lasting heating and generating a stronger predawn heating effect. Considering the important impact of AMFS, predawn heating will not only occur near the solstices but also occur at other seasons even at the equinoxes with large AMFS values.

The influence of LMF on predawn heating is primarily sourced from the heating loss due to collisions between photoelectrons and the surrounding plasma during their trans-hemispheric transportation. The longer the LMF is, the greater the integrated electron content along the field line, leading to greater loss of photoelectrons during their trans-hemispheric transportation. Consequently, fewer electrons reach the conjugated hemisphere, resulting in a weaker heating effect.

Although the AMFS can enhance heating effect, however, there is a ceiling to this heating enhancement, which we can call the saturation effect. When the LMF is longer than 8000 km and the AMFS is larger than about 35 degrees, even the AMFS continues to increase, the heating effect will no longer increase. Similarly, in the case of a small AMFS, the impediment effect of a longer LMF on predawn heating is also saturated.

4. Summary and Conclusions

Utilizing a substantial dataset of topside ionosphere ion temperatures measured by the Rocsat-1 satellite, we have established a global ion temperature model for middle and low latitudes using a gridded approach. The median error between the model results and observations is 58.6K. Subsequently, we employed the established empirical ion temperature model to simulate the global distribution of topside ionosphere ion temperatures across different seasons.

Based on these simulation results, we focused on the crucial controlling factors of the predawn heating effect. Previous research has considered the length of magnetic field lines to be an important factor. In this study, we proposed for the first time that the angle between the projection of the magnetic field line on the horizontal plane and the sunrise line is another key factor controlling predawn heating. Accordingly, we investigated quantitatively the relationship between the predawn heating effect and the AMFS using the model results and examined the LMF's influence. The results indicate that the predawn ion heating is influenced by the combined effect of the AMFS and the LMF. Our study further suggests that an increase in AMFS strongly promotes predawn heating, and the heating efficiency gradually diminishes with the increase in the LMF. Similarly, the longer the LMF is, the weaker the predawn heating effect is. the influence of the LMF on the predawn ion temperature enhancement is increased as AMFS increases.

By comprehensively considering the combined effect of AMFS and the LMF, we statistically analyzed the results of ion heating under different LMF values (2,000 - 10,000 km) and different AMFS values (5° - 50°). We found that when the LMF is about 4000 km and the AMFS is around 30 degrees, the combined effect of AMFS and the LMF on the predawn heating effect reaches its maximum. At the same time, the influence of both AMFS and LMF exhibit the saturation effect.

Data Availability Statement

The Kp geomagnetic index and the F10.7 solar radio flux can be downloaded from GFZ Potsdam on (https://kp.gfz-potsdam.de/en/data). The observed Rocsat-1 satellite data was provided by National Central University of Taiwan, which can be downloaded from (https://spdf.gsfc.nasa.gov/pub/data/formosat-rocsat/formosat-1/ipei/).

Acknowledgments

This research was supported by the B-type Strategic Priority Program of the Chinese Academy of Sciences (XDB41000000), National Natural Science Foundation of China (42274223), Youth Innovation Promotion Association CAS.

Reference

A, E., Zhang, D., Ridley, A. J., Xiao, Z., & Hao, Y. (2012). A global model: Empirical orthogonal function analysis of total electron content 1999–2009 data. Journal of Geophysical Research, 117, A03328. https://doi.org/10.1029/2011JA017238

Alken, P., Thébault, E., Beggan, C. D., Amit, H., Aubert, J., et al. (2021). International Geomagnetic Reference Field: the thirteenth generation. Earth, Planets and Space, 73, 49. https://doi.org/10.1186/s40623-020-01288-x

Banks, P. M., and G. Kockarts. "Aeronomy, part B." (1973): 282.

Brace, L. H., & Theis, R. F. (1981). Global empirical models of ionospheric electron temperature in the upper F-region and plasmasphere based on in situ measurements from the Atmosphere Explorer-C, ISIS-1 and ISIS-2 satellites. Journal of atmospheric and Terrestrial physics, 43(12), 1317-1343. doi: 10.1016/0021-9169(81)90157-4.

Carlson Jr, H. C. (1966). Ionospheric heating by magnetic conjugate-point photoelectrons. Journal of Geophysical Research, 71(1), 195-199. doi: 10.1029/JZ071i001p00195.

Chao, C. K., Su, S. Y., & Yeh, H. C. (2003). Presunrise ion temperature enhancement observed at 600 km low-and mid-latitude ionosphere. Geophysical research letters, 30(4). doi: 10.1029/2002GL016268.

Chao, C. K., Su, S. Y., Huba, J. D., & Oyama, K. I. (2010). Modeling the presunrise plasma heating in the low-to midlatitude topside ionospheres. Journal of Geophysical Research: Space Physics, 115(A9). doi: 10.1029/2009JA014923.

Hanson, W. B., Sanatani, S., Zuccaro, D., & Flowerday, T. W. (1970). Plasma measurements with the retarding potential analyzer on Ogo 6. Journal of Geophysical Research, 75(28), 5483-5501. doi: 10.1029/JA075i028p05483.

Heelis, R. A., & Hanson, W. B. (1980). Interhemispheric transport induced by neutral zonal winds in the F region. Journal of Geophysical Research: Space Physics, 85(A6), 3045-3047. doi: 10.1029/JA085iA06p03045.

Huang, C. S. (2023). Identification of penetration and disturbance dynamo electric fields and their effects on the generation of equatorial plasma bubbles. Journal of Geophysical Research: Space Physics, 128(11), e2023JA031766. doi:

10.1029/2023JA031766

Kakinami, Y., Balan, N., Liu, J. Y., & Oyama, K. I. (2010). Predawn ionospheric heating observed by Hinotori satellite. Journal of Geophysical Research: Space Physics, 115(A1). doi: 10.1029/2009JA014334.

Köhnlein, W. (1986). A model of the electron and ion temperatures in the ionosphere. Planetary and space science, 34(7), 609-630. doi: 10.1016/0032-0633(86)90039-5 .

Kwei, M. W., & Nisbet, J. S. (1968). Presunrise heating of the ionosphere at Arecibo due to conjugate point photoelectrons. Radio Science, 3(7), 674-679. doi: 10.1002/rds196837674.

Le, H., Liu, L., Ding, F., Ren, Z., Chen, Y., Wan, W., ... & Hu, L. (2010). Observations and modeling of the ionospheric behaviors over the east Asia zone during the 22 July 2009 solar eclipse. Journal of Geophysical Research: Space Physics, 115(A10). doi: 10.1029/2010JA015609.

Le, H., Liu, L., Ren, Z., Chen, Y., & Zhang, H. (2020). Effects of the 21 June 2020 solar eclipse on conjugate hemispheres: A modeling study. Journal of Geophysical Research: Space Physics, 125(11), e2020JA028344. doi: 10.1029/2020JA028344.

Le, H., Liu, L., Yue, X., & Wan, W. (2008). The midlatitude F2 layer during solar eclipses: Observations and modeling. Journal of Geophysical Research: Space Physics, 113(A8). doi: 10.1029/2007JA013012.

Oyama, K. I., Balan, N., Watanabe, S., Takahashi, T., Isoda, F., GJ, B., & Oya, H. (1996b). Morning overshoot of Te enhanced by downward plasma drift in the equatorial topside ionosphere. Journal of geomagnetism and geoelectricity, 48(7), 959-966. doi: 10.5636/jgg.48.959.

Oyama, K. I., Watanabe, S., Su, Y., Takahashi, T., & Hirao, K. (1996a). Season, local time, and longitude variations of electron temperature at the height of∼ 600 km in the low latitude region. Advances in Space Research, 18(6), 269-278. doi: 10.1016/0273-1177(95)00936-1.

Richards, P. G., & Torr, D. G. (1986). Thermal coupling of conjugate ionospheres and the tilt of the Earth's magnetic field. Journal of Geophysical Research: Space Physics, 91(A8), 9017-9021. doi: 10.1029/JA091iA08p09017.

Truhlík, V., Bilitza, D., Kotov, D., Shulha, M., & Třísková, L. (2021). A global empirical model of the ion temperature in the ionosphere for the international reference ionosphere. Atmosphere, 12(8), 1081. doi: 10.3390/atmos12081081.

Venkatraman, S., & Heelis, R. (1999). Longitudinal and seasonal variations in nighttime plasma temperatures in the equatorial topside ionosphere during solar maximum. Journal of Geophysical Research: Space Physics, 104(A2), 2603-2611. doi: 10.1029/1998JA900109.

Figure Captions

Figure 1. The left panel shows the ion temperature error, and the median error of the model is 58.6K. The right panel is the count bin figure, and the black line represents the fitting line between the observed and model results, with a slope of 1.0041.

Figure 2. Figure 2a-c illustrates the global distribution of ion temperatures at certain Universal Time (UT) at the June solstice and March equinox, when the altitude is 600km and F107 is 140. Figure 2d elaborates the definition and calculation of AMFS. The magenta line is the sunrise line, and the black line is the projection of the magnetic field line on the horizontal plane. L_{M1} and L_{M2} indicate the points of the same magnetic latitude in the northern and southern hemispheres. L_{R1} and L_{R2} indicate the position of sunrise at the corresponding magnetic latitude. A1 and A2 indicate the points at which predawn heating is calculated in the northern and southern hemispheres.

Figure 3. The relationship between AMFS and the temperature difference between the northern and southern hemispheres, within different ranges of LMF (from 2000-10000 km, with a span of plus or minus 10% before and after). The red line represents the fitting straight line, with k being the slope of the straight line.

Figure 4. The relationship between the LMF and the temperature difference between the northern and southern hemispheres in different AMFS, and other descriptions are the similar as Figure 3.

Figure 5. The combined effect of the LMF and AMFS on the predawn heating effect.

Figure

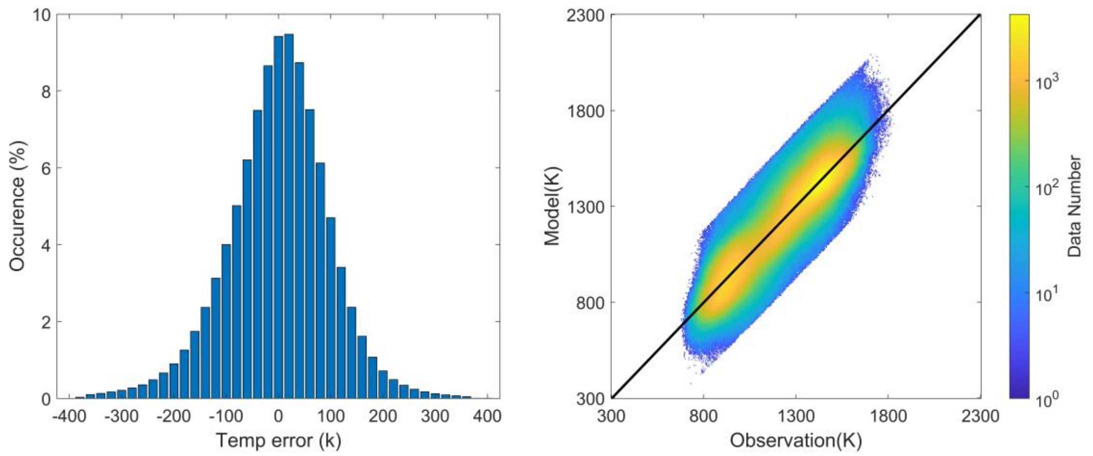

Figure 1. The left panel shows the ion temperature error, and the median error of the model is 58.6K. The right panel is the count bin figure, and the black line represents the fitting line between the observed and model results, with a slope of 1.0041.

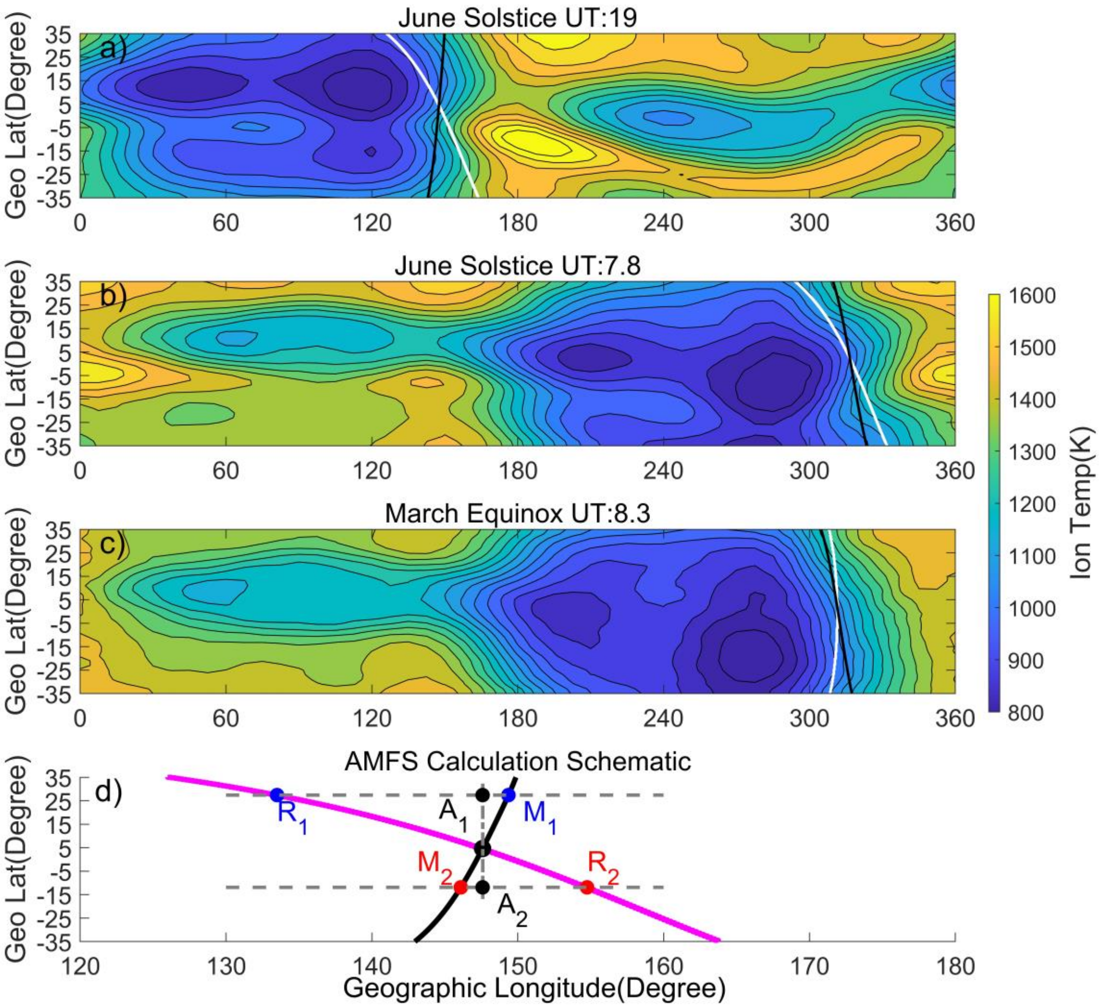

Figure 2. Figure 2a-c illustrates the global distribution of ion temperatures at certain Universal Time (UT) at the June solstice and March equinox, when the altitude is 600km and F107 is 140. Figure 2d elaborates the definition and calculation of AMFS. The magenta line is the sunrise line, and the black line is the projection of the magnetic field line on the horizontal plane. LM1 and LM2 indicate the points of the same magnetic latitude in the northern and southern hemispheres. LR1 and LR2 indicate the position of sunrise at the corresponding magnetic latitude. A1 and A2 indicate the points at which predawn heating is calculated in the northern and southern hemispheres.

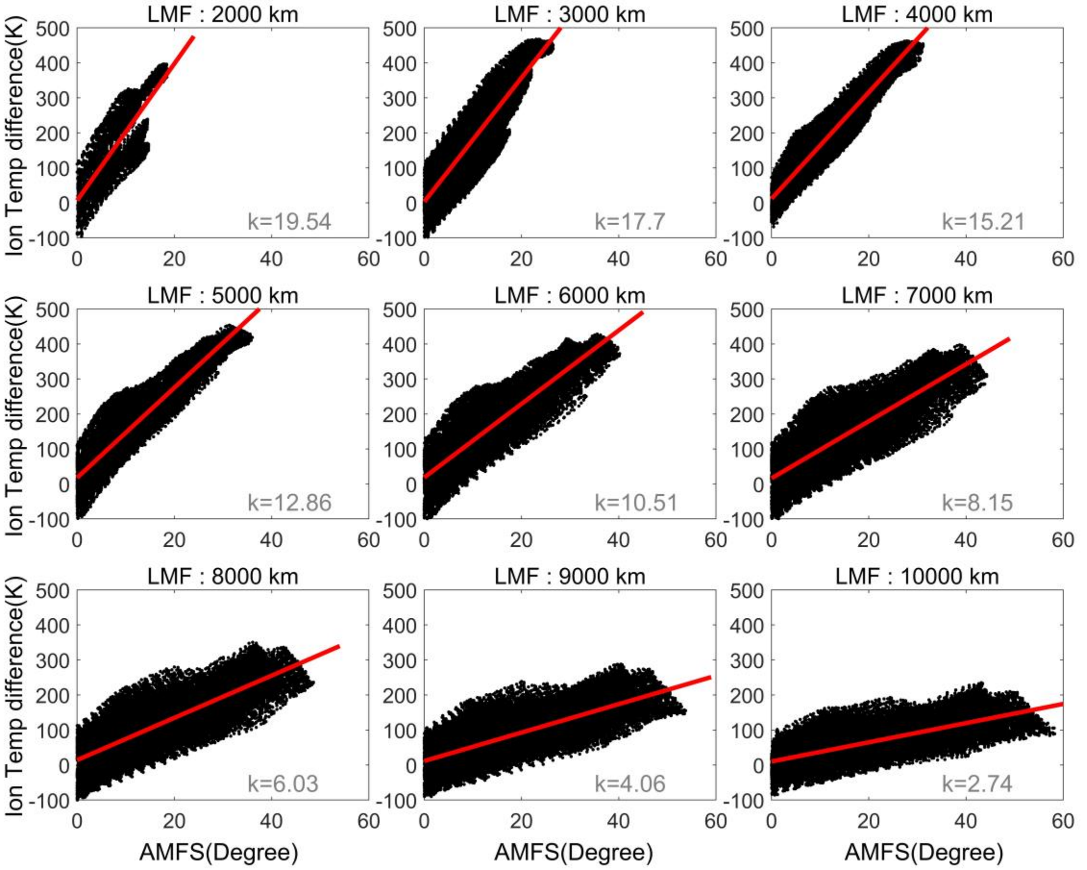

Figure 3. The relationship between AMFS and the temperature difference between the northern and southern hemispheres, within different ranges of LMF (from 2000-10000 km, with a span of plus or minus 10% before and after). The red line represents the fitting straight line, with k being the slope of the straight line.

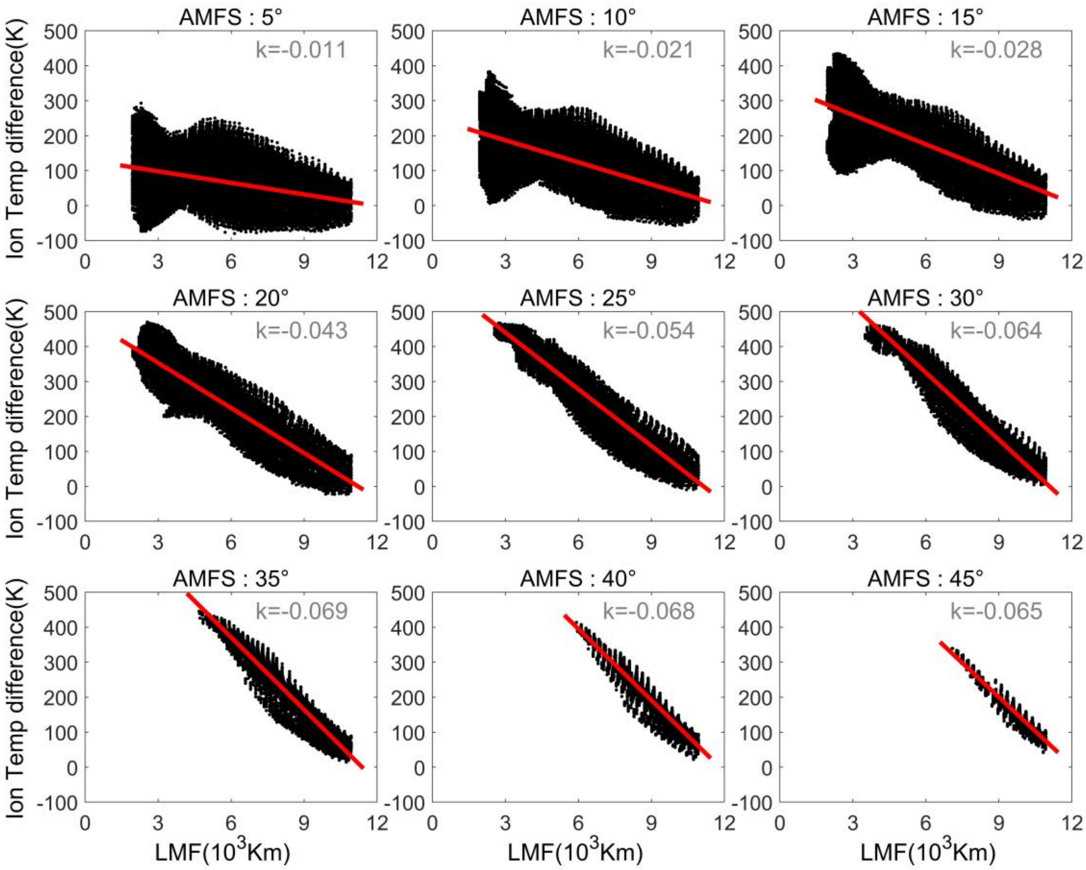

Figure 4. The relationship between the LMF and the temperature difference between the northern and southern hemispheres in different AMFS, and other descriptions are the similar as Figure 3.

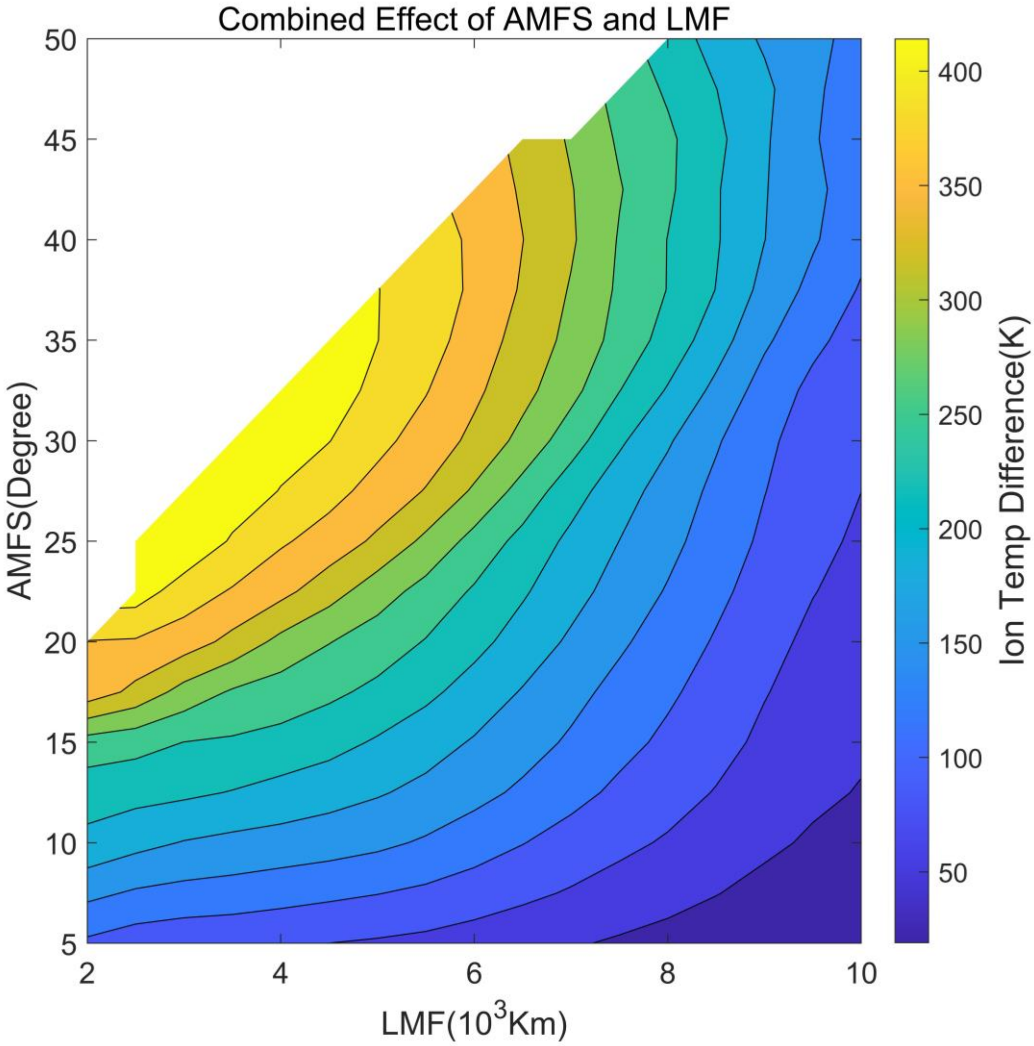

Figure 5. The combined effect of the LMF and AMFS on the predawn heating effect.